processes

MDPI

Article

DEM Study on the Segregation of a Non-Spherical Intruder in a Vibrated Granular Bed

Jinpeng Qiao [1], Kejun Dong [2,*] and Chenlong Duan [1,*]

[1] Key Laboratory of Coal Processing and Efficient Utilization of Ministry of Education, School of Chemical Engineering and Technology, China University of Mining and Technology, Xuzhou 221116, China; joe.9911@cumt.edu.cn

[2] Centre for Infrastructure Engineering, School of Engineering, Western Sydney University, Sidney, NSW 2751, Australia

* Correspondence: Kejun.Dong@westernsydney.edu.au (K.D.); clduan@cumt.edu.cn (C.D.)

Abstract: The segregation process of a single large intruder in a vibrated bed of small particles has been widely studied, but most previous studies focused on spherical intruders. In this work, the discrete element method was used to study the effects of vibration conditions and intruder shape on the dimensionless ascending velocity (v_a) of the intruder. The intruder was in a prolate shape with aspect ratio varied but its equivalent diameter fixed. Three equivalent diameters, namely volume-equivalent diameter, surface-area-equivalent diameter, and Sauter diameter, were used. It was found that v_a increases and then decreases with the rise of the dimensionless vibration amplitude (A_d) and the dimensionless vibration frequency (f_d), and v_a increases with the decrease of the sphericity of the intruder (Φ). Moreover, the porosity variation in the vibrated bed and the granular temperature were analyzed, which can be linked to the change of v_a. It was further found that v_a can be uniformly correlated to $A_d \cdot f_d^{0.5}$, while the critical change of the response of v_a to A_d and f_d occurs at $\Gamma = 4.83$, where Γ is the vibration intensity. Based on these findings, a piecewise equation was proposed to predict v_a as a function of A_d, f_d, and Φ.

Keywords: non-spherical particle; ascending velocity; segregation; discrete element method

check for updates

Citation: Qiao, J.; Dong, K.; Duan, C. DEM Study on the Segregation of a Non-Spherical Intruder in a Vibrated Granular Bed. *Processes* **2021**, *9*, 448. https://doi.org/10.3390/pr9030448

Academic Editor: Alberto Di Renzo

Received: 1 February 2021
Accepted: 26 February 2021
Published: 2 March 2021

Publisher's Note: MDPI stays neutral with regard to jurisdictional claims in published maps and institutional affiliations.

Copyright: © 2021 by the authors. Licensee MDPI, Basel, Switzerland. This article is an open access article distributed under the terms and conditions of the Creative Commons Attribution (CC BY) license (https://creativecommons.org/licenses/by/4.0/).

1. Introduction

The segregation of granular mixtures under vibration is often encountered in various industrial processes [1–3]. A good understanding of the segregation mechanism can help the optimization and control of the related processes. The research of such a phenomenon often starts with the segregation of a single large intruder in an otherwise homogeneous granular bed of small particles [4–6]. Under vibration, the large intruder normally ascends in the granular bed. Based on the statistical analysis on the interaction between the intruder and the surrounding small particles, several kinds of segregation mechanisms have been proposed for such an ascending phenomenon, including void filling, global convection, etc. [7–11]. In addition, in different experimental and numerical studies, the ascending velocity, which is the average velocity of the intruder in its rising process from the bottom to the top of the vibrated bed, was often modeled against different controlling variables [12].

The literature indicates the dependence of the ascending velocity on the following variables: particle properties including the density ratio (ρ_r) [13–15] and the size ratio (d_r) [16,17]; particle bed features including the aspect ratio [18], friction [19], and filling height [20]; and vibration conditions including vibration amplitude [21], frequency [12], and intensity [10,22]. For particle properties, a general observation is that the increase of the size ratio and density ratio both increase the ascending velocity [17,20,22]. The shape of the container would affect the granular flow direction [18,23] and control the particle convection [24]. In addition, with or without friction between particles and the wall, the rise time of the intruder is rather different [25]. For vibration conditions, the increase of

vibration amplitude (A) will increase the ascending velocity of the intruder [21], while the increase of vibration frequency (f) generally decreases the ascending velocity [26].

The previous studies, however, were focused on spherical intruders. The non-spherical intruder has not been studied much yet. The intruder shape was once reported to have an insignificant effect on the segregation of granular mixtures [26]. However, more recent studies show that the shape of particles is important to their motions in particle mixtures when subject to shearing vibrations [27,28]. As listed in Table 1, there are different mathematical models for the segregation rate of spherical intruders proposed in the literature. However, similar models for non-spherical intruders have not been seen to the best of our knowledge. Besides, in most models the vibration intensity Γ ($\Gamma = 4\pi^2 A f^2/g$) was assumed as a key controlling variable, and under the same Γ, the influence of A and f on segregation rate was shown to be monotonic. However, the non-monotonic response of segregation rate to A and f was observed in some recent studies [29,30], which indicates that this segregation should be studied in a wider range of vibration conditions and intruder shapes.

Table 1. List of models for the ascending of a spherical intruder in a vibrated bed of small particles.

Reference	Methodology	Investigated Parameters	Mathematical Model
Liffman et al. [22]	Experiment 2D	A = 15 mm f = 4–5 Hz Γ = 0.6–11	$v_a = \Gamma a_d \sqrt{\frac{\rho_d a_p g}{2\sqrt{6}\beta\rho_b[cy^2+b\lvert y\rvert+a]}}$
Jiang et al. [31]	Experiment 3D	f = 60 Hz Γ = 2.5–11	$T_{seg} = K\frac{H_{bed}f^3}{g^2(\Gamma^2-1)^2} + \varphi$
Peng et al. [32]	Experiment 3D	f = 60 Hz Γ = 1.5–11	$T_{seg} = \frac{a}{b\Gamma+c}$
Liu et al. [33]	Experiment 3D	f = 60 Hz Γ = 2–11	$T_{seg} = \frac{4\pi^2 H_{bed}f^2}{k\cdot\rho_{ratio}\cdot g\cdot(\Gamma-\Gamma_c)}$

T_{seg}—total segregation time; v_a—ascend velocity of intruder; Γ_c—minimum vibration intensity; Γ—vibration intensity; a_d—radius of disk; ρ_b—bulk density of bed; β—granular friction coefficient; a_p—average radius of bulk particles; ρ_d—the mass density of the disk; K, k, φ, c, a, b—correction coefficient; H_{bed}—bed height; f—vibration frequency; ρ_{ratio}—density ratio of the large particle to the small particle.

In this paper, the segregation process of a single non-spherical intruder is studied by the discrete element method (DEM). The effects of vibration amplitude and frequency on the defined dimensionless ascending velocity are investigated. Based on the simulation results, an equation is proposed to uniformly link the ascending velocity to the vibration conditions and the shape of the intruder, and particularly the non-monotonic change of the ascending velocity with the vibration conditions is also uniformly considered. These results provide new insights into particle segregation under vibration and new dimensionless models to predict the segregation speed, which could be useful for modeling powder mixing and segregation.

2. Materials and Methods

2.1. Model Description

The discrete element method (DEM) has been proven as an effective technology to study granular mixtures at a particle scale [34–37]. Considering computational efficiency and successful experience according to previous literature, the typical Hertz–Mindlin particle contact model is adopted in this work. Based on Newton's laws of motion, the translational motion and rotational motion of particle i are, respectively, determined by

$$m_i \frac{dv_i}{dt} = m_i g + \sum_{j=1}^{n_i} \left(F_{n,ij} + F_{t,ij}\right) \quad (1)$$

$$I_i \frac{d\omega_i}{dt} = \sum_{j=1}^{n_i} \left(T_{t,ij} + T_{r,ij}\right) \quad (2)$$

where v_i, ω_i, and I_i are the translational and angular velocities, and the moment of inertia of particle i, respectively; g is the gravitational acceleration and t is time; m_i is mass of particle I; n_i is the total number of particles in contact with particle i; $F_{n,ij}$ is the normal contact force, including the normal-contact force and the normal-damping force. $F_{t,ij}$ is the tangential contact force, including the tangential contact and the tangential damping force. The commercial software EDEM 2018 (DEM Solutions Ltd., Edinburgh, United Kingdom) was used to conduct the DEM simulations, and the details of the force models can be found in the manual [38].

2.2. Simulation Conditions and Validation

A 3D cuboid "container" without physical walls was adopted in this research, as shown in Figure 1a. The bed size was 20 × 20 × 60 mm and periodic boundary conditions (PBCs) were applied along the X-axis and Y-axis directions, which can prevent granular convection induced by the side wall during the vibration [24,39] and its effect on the ascending of the intruder [29]. The initial undisturbed bed consisted of one single non-spherical large intruder in an otherwise homogeneous spherical granular bed with the total bed height $H_{bed} \approx 30 \cdot d_s$, where d_s is the diameter of small particles. The parameters used in the simulations are given in Table 2. Continuous and sinusoidal vibrations with wide range of frequency f and amplitude A were applied to the bottom wall along the Z-axis. The non-spherical intruder was in a prolate shape and was initially placed with its long axis aligning with the Z-axis direction. According to our observations, the orientation of the intruder had slight changes during the ascending process, and the average angle between its long axis and the vibration direction was less than 15 degrees, as shown in Figure 1b.

It should be noted that there are different ways to consider the size of a non-spherical particle. In the present research, the equivalent diameter of a non-spherical intruder was calculated in three ways; namely, volume equivalent diameter (d_{Vol}), area equivalent diameter (d_{Area}), and Sauter diameter (d_{Sau}), which are respectively given by

$$d_{Vol} = \sqrt[3]{6V/\pi} \tag{3}$$

$$d_{Area} = \sqrt{S/\pi} \tag{4}$$

$$d_{Sau} = {d_{Vol}}^3 / {d_{Area}}^2 \tag{5}$$

where V and S are, respectively, the volume and surface of the non-spherical intruder. The axial sizes of the non-spherical intruders of different sphericities are listed in Table 3.

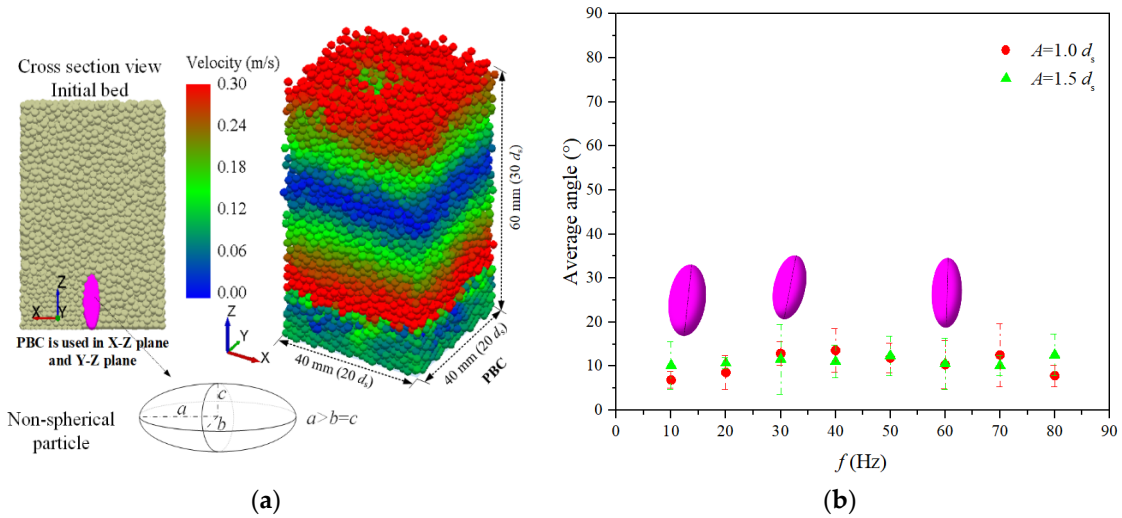

Figure 1. (**a**) Schematic of the simulated single non-spherical intruder in a vibrated bed of small particles; (**b**) average angle between the intruder's long axis and the vibration direction—the error bar shows the variation range of the acute angle between the intruder's long axis and the Z-axis.

Table 2. List of parameters used in the simulations.

Parameters	Value of Parameter
Poisson's ratio of particles	0.25
Poisson's ratio of container base	0.29
Young's modulus of particles (Pa)	2.01×10^5
Young's modulus of container base (Pa)	2.55×10^{10}
Coefficient of restitution: particle–particle	0.5
Coefficient of static friction: particle–particle	0.5
Coefficient of rolling friction: particle–particle	0.01
Coefficient of restitution: particle–base	0.5
Coefficient of static friction: particle–base	0.5
Coefficient of rolling friction: particle–base	0.01
Intruder equivalent diameter, d_l (mm)	6.0
Intruder shape	Ellipsoid, spherical
Intruder aspect ratio, a/b	varies in [1.0, 5.75]
Diameter of small particles, d_s (mm)	2
Diameter ratio, $d_r = d_l/d_s$	3.0
Particle density: Large (Intruder), ρ_l (kg/m^3)	2500
Particle density: Small, ρ_s (kg/m^3)	2500
Density ratio, ρ_l/ρ_s	1.0
Number of large particles (intruder)	1
Number of small particles	15,200
Vibration amplitude A (mm)	1–5 ($0.5 \cdot d_s$–$2.5 \cdot d_s$)
Vibration frequency f (Hz)	20–80

Table 3. Axial sizes of non-spherical intruders used in simulation.

Equivalent Ways (d_l = 6 mm)	Axial Size (mm)	Sphericity, Φ							
		0.97	**0.93**	**0.89**	**0.85**	**0.81**	**0.78**	**0.73**	**0.70**
d_{Vol}	a	3.93	4.76	5.53	6.24	6.91	7.56	8.77	9.63
	b	2.62	2.38	2.21	2.08	1.97	1.89	1.75	1.67
d_{Area}	a	3.88	4.59	5.20	5.74	6.23	6.68	7.50	8.06
	b	2.59	2.30	2.08	1.91	1.78	1.67	1.50	1.40
d_{Sau}	a	4.04	5.13	6.24	7.38	8.52	9.67	11.98	13.72
	b	2.69	2.57	2.50	2.46	2.43	2.42	2.40	2.39

The simulation time step was set to 9.06×10^{-5} s, which is 20% of the Rayleigh time step. The simulation time for each case was over 25 s. To validate the model, the simulated results were compared to the literature. The simulated ascending process is shown in Figure 2. It can be seen that the height–time curve simulated by our model is in good agreement with that of the physical experiments [11], as shown in Figure 2a. In addition, as shown in Figure 2b, the simulated total ascending time as a function of the vibration amplitude is in good agreement with the experiment results [11]. The good agreement can validate the DEM model.

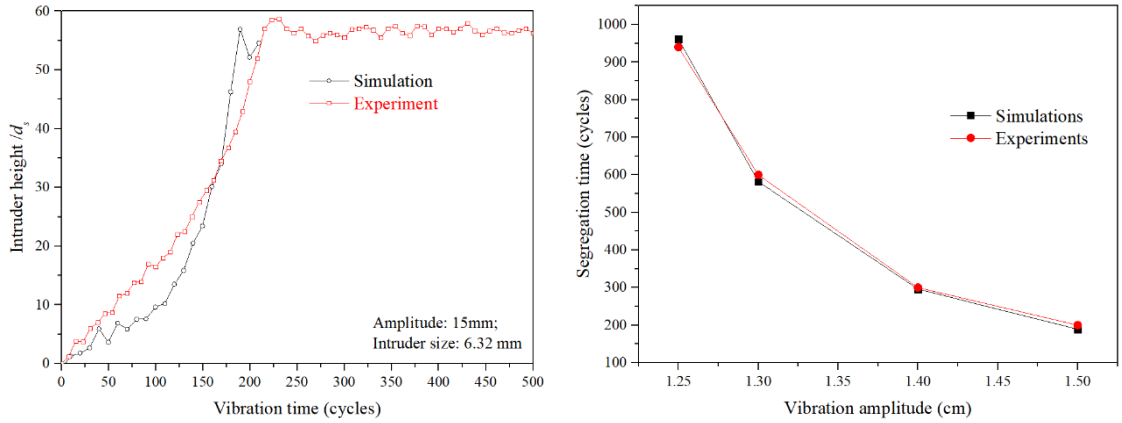

Figure 2. Comparison of simulation results and experiment results in Nahmad-Molinari et al. [11]: (**a**) the ascending height of the intruder as a function of vibration time; (**b**) the segregation time as a function of vibration amplitude under f = 7.5 Hz.

2.3. Evaluation Indexes

In this research, the ascending velocity of the intruder, v_a, is defined as the average vertical displacement of the intruder per oscillation cycle [29]:

$$v_{\mathrm{a}} = \frac{\Delta H / d_s}{T} \tag{6}$$

where ΔH is the vertical distance traveled by the intruder in the ascending process, mm; d_{s} is the size of small particles; T is the number of oscillation cycles in the ascending process. It is worth noting that v_a obtained in Equation (6) is an average value but is reasonable to represent the ascending behavior. As shown in Figure 3, with different vibration amplitudes, the ascending height is generally in linear dependence to the vibration time, and the fluctuations are observed only when the height of the intruder is close to the top of the bed.

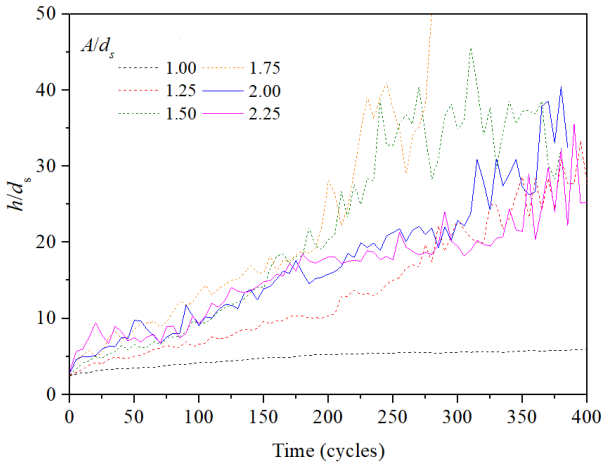

Figure 3. The vertical position of the intruder in the ascending process under different vibration amplitudes. d_{Sau} = 6 mm, f = 20 Hz, d_l/d_s = 3.0.

3. Results and Discussion

3.1. Effects of Vibration Amplitude on v_a

As shown in Figure 4a,b, v_a of a non-spherical intruder increased first and then decreased with dimensionless vibration amplitude A_d ($A_d = A/d_{\mathrm{s}}$), and the critical change occurred at A_d = 1.5. In addition, v_a of the non-spherical intruder of aspect ratio a/b = 3.0 was larger than that of a/b = 2.0. Additionally, regardless of which equivalent diameter was used, the non-spherical intruder's ascending velocity was much higher than that of a

spherical intruder (a/b = 1.0), and the velocity difference increased with the increase of the aspect ratio, as shown in Figure 4c.

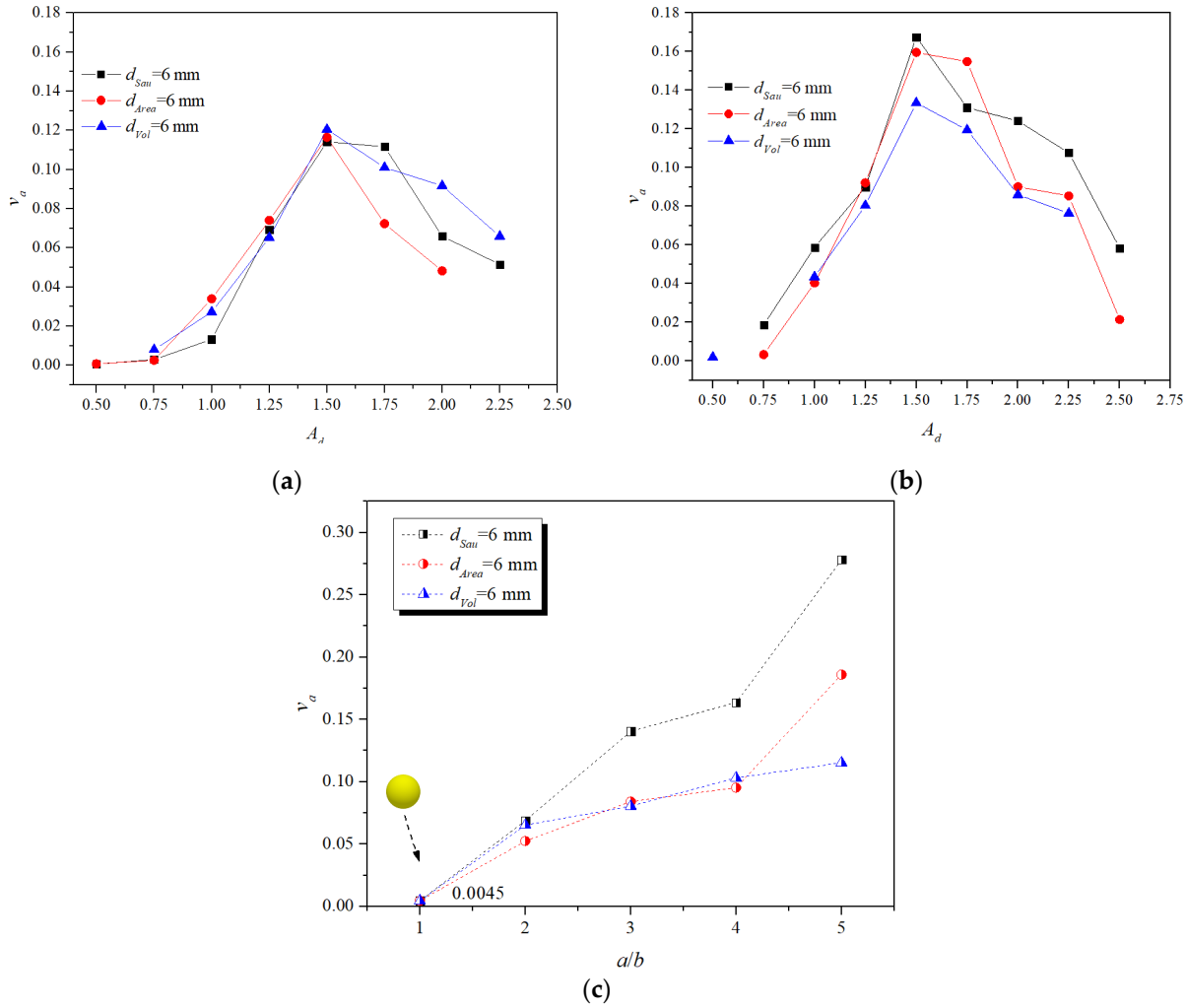

Figure 4. (**a**) v_a as a function of A with f = 20 Hz and a/b = 2.0; (**b**) v_a as a function of A with f = 20 Hz and a/b = 3.0; (**c**) v_a as a function of a/b, with f = 20 Hz and $A = 1.25 \cdot d_s$. The yellow sphere means the intruder of a/b = 1.0.

From Figure 3, it can be seen that in the ascending process of the intruder, the intruder actually experiences an alternating rise and fall. This is understandable as in each vibration cycle, the bed is lifted in the first half cycle, then the bottom wall moves downwards and so the particles also fall. Therefore, the filling of small particles in the void region underneath the big intruder is acknowledged as one of the major mechanisms for the overall ascending of the intruder [21], and the change of v_a with A_d is probably also related to this mechanism. The increase of v_a with increasing A_d has also been observed for a spherical intruder by Ahmad et al. [26] and by Rosato et al. [21]. As explained by Rosato et al., such an increase can be attributed to the fact that larger vibration amplitude will cause more voids which promote the filling of small particles beneath the large intruder, and thus accelerate the ascending. This explanation is also applicable to the ascending of a non-spherical intruder.

However, when $A > 1.5 \cdot d_s$, a further increase of vibration amplitude led to a decrease of v_a. Such critical change can be linked with the structural changes in the vibrated bed. For spherical particles, Hsiao et al. [30] found that the segregation rate of a group of large intruders in a vibrated bed of small particles undergoes a nonmonotonic change with increasing vibration intensity. The primary cause for the critical change is that a too high vibration intensity can create very large voids, which let larger intruders fall down rather

than ascend. When vibration intensity is too high, the bed stops further expanding and the voids are so large that the probabilities for the larger intruder and smaller particles to fall down are equal, thus segregation no longer occurs. In addition, a later study [29] on the segregation of a single spherical intruder further proved that the ascending velocity has a strong dependence on the porosity variation of the particle bed.

Therefore, the non-monotonic response caused by A_d for a non-spherical intruder can be linked to the variations of bed porosity (ε), which was investigated here. The porosity was calculated by dividing the particle bed into several horizontal layers with vertical thickness of $3.5 \cdot d_s$, and the porosity of each layer was calculated. The porosity variation ($\Delta\varepsilon$) is defined as the difference between the maximum and minimum of the bed porosity within one oscillation period, and the value is averaged over ten full-oscillation cycles. Figure 5 shows the porosity variation for different layers. Generally, $\Delta\varepsilon$ increased first and then decreased with the continuous increase of A_d, and the critical changes occurred when A_d = 1.5. The comparable change of v_a to that of $\Delta\varepsilon$ hints that increasing the vibration amplitude would cause a larger $\Delta\varepsilon$, which gives small particles more opportunities to fill voids beneath the intruder, thus accelerating the ascending. However, when vibration is too extensive, $\Delta\varepsilon$ reduces and the void filling becomes less efficient, and hence the ascending slows down.

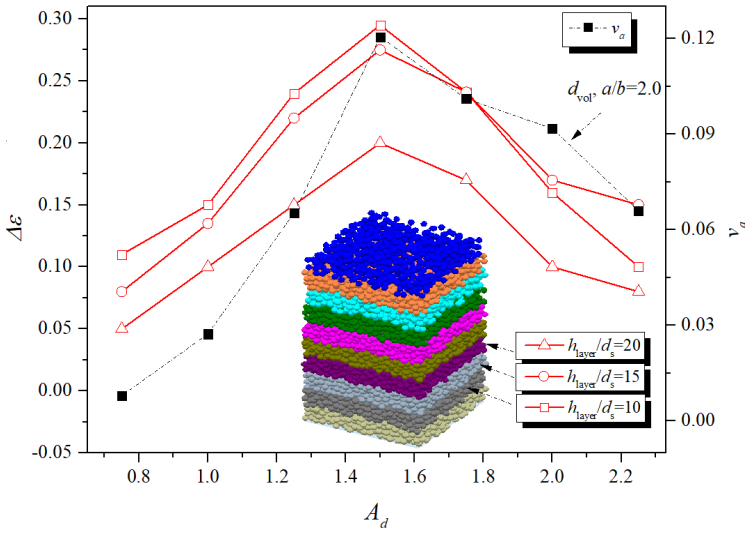

Figure 5. Influence of A on $\Delta\varepsilon$ for different bed layers (○, □, and △) and v_a (■), f = 20 Hz.

Similarly, the increase of v_a with the increase of the aspect ratio of the intruder can also be linked to the change of porosity variation at different bed heights. Figure 6a shows that $\Delta\varepsilon$ varied significantly with bed height, and higher layers showed smaller $\Delta\varepsilon$. Therefore, when the centers of intruders with different aspect ratios are at the same height, as shown in Figure 6b, the elongated shape of the non-spherical intruder enables its lower-end to reach a deeper bed, where the void filling is more efficient. The more efficient void filling brings the non-spherical intruder of a larger aspect ratio a faster rise.

3.2. Effects of Vibration Frequency on v_a

Similar to the effect of vibration amplitude, Figure 7 shows that, for both the spherical and the non-spherical intruders, the ascending velocity also increased and then decreased with increasing dimensionless vibration frequency. Comparably, non-spherical intruders have much higher v_a than that of the spherical intruder. Here the dimensionless frequency is defined as $f_d = f \cdot (2 \cdot d_s / g)^{0.5}$.

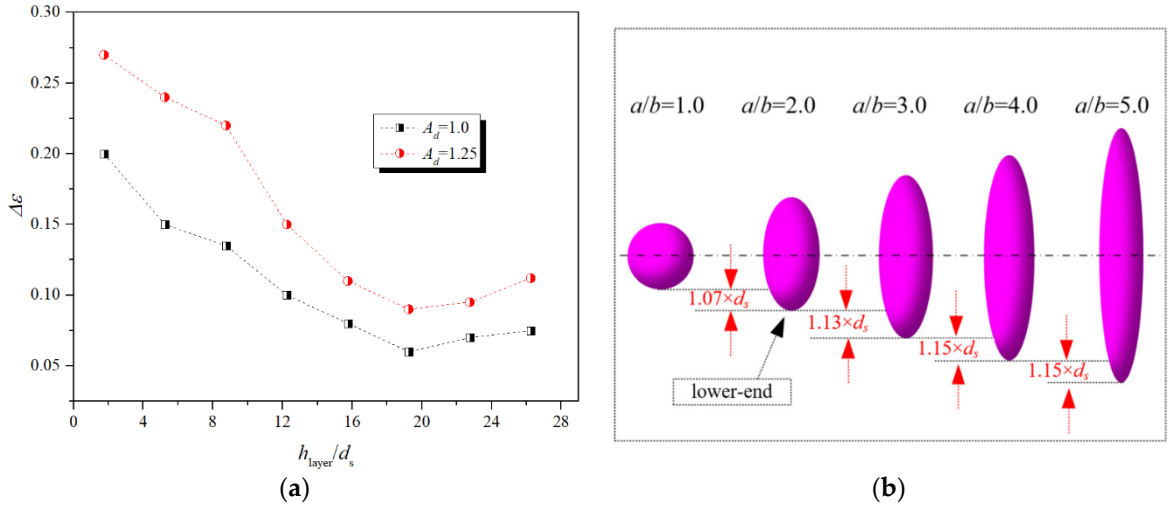

Figure 6. (**a**) Δε varies with bed layer; (**b**) a schematic of intruders with different aspect ratios.

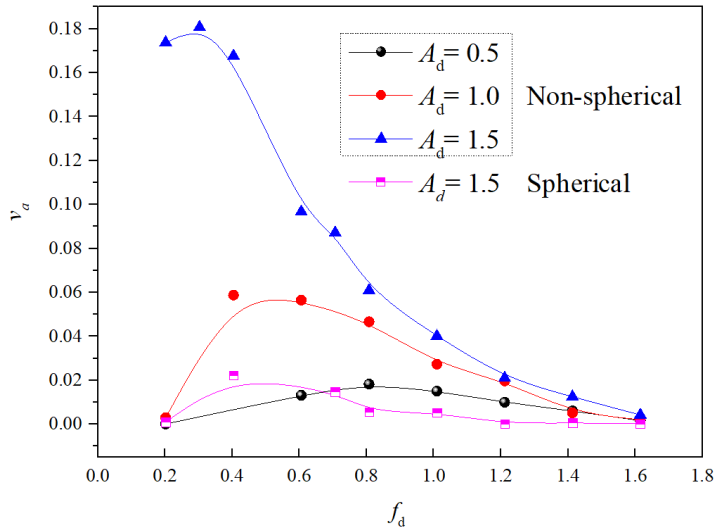

Figure 7. The influence of f_d on v_a for the spherical intruder (d_l = 6 mm) and the non-spherical intruder (d_{Sau} = 6 mm, a/b = 3.0).

Such a non-monotonic dependence was also observed in our previous research on binary mixtures, when A is fixed, and f varies [40]. The previous explanations of the influence of f were based on its impact on granular convection intensity [12,40]. However, as shown in Figure 8, there is no granular convection in the present research.

Similar to the above discussion on the effect of vibration amplitude, the non-monotonic change of v_a may also be related to the change of bed porosity. As shown in Figure 9a, Δε of bed layer at a height of $20 \cdot d_s$ increased first and then decreased with f_d, which is consistent with the trend of v_a. The change in Δε has a significant influence on filling interstices for small particles, and an increase or decrease of Δε would accordingly promote or suppress the ascending velocity. Besides, it is worth noting that the small particles can change from a disordered structure to an ordered structure under certain vibration conditions, which has been reported in our recent studies [41,42]. This can also impose an important influence on the intruder's ascending behavior and deserves further studies.

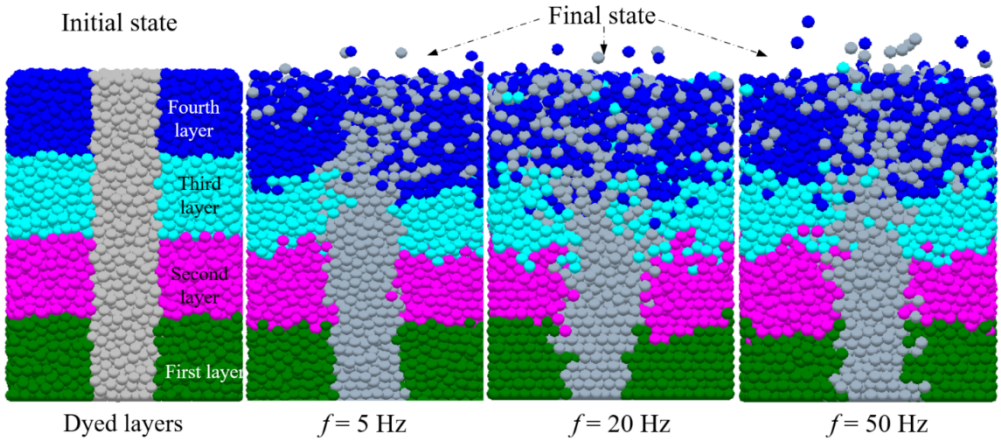

Figure 8. The distribution of small particles at initial dyed layers and final layers after vibration of A =2·d_s.

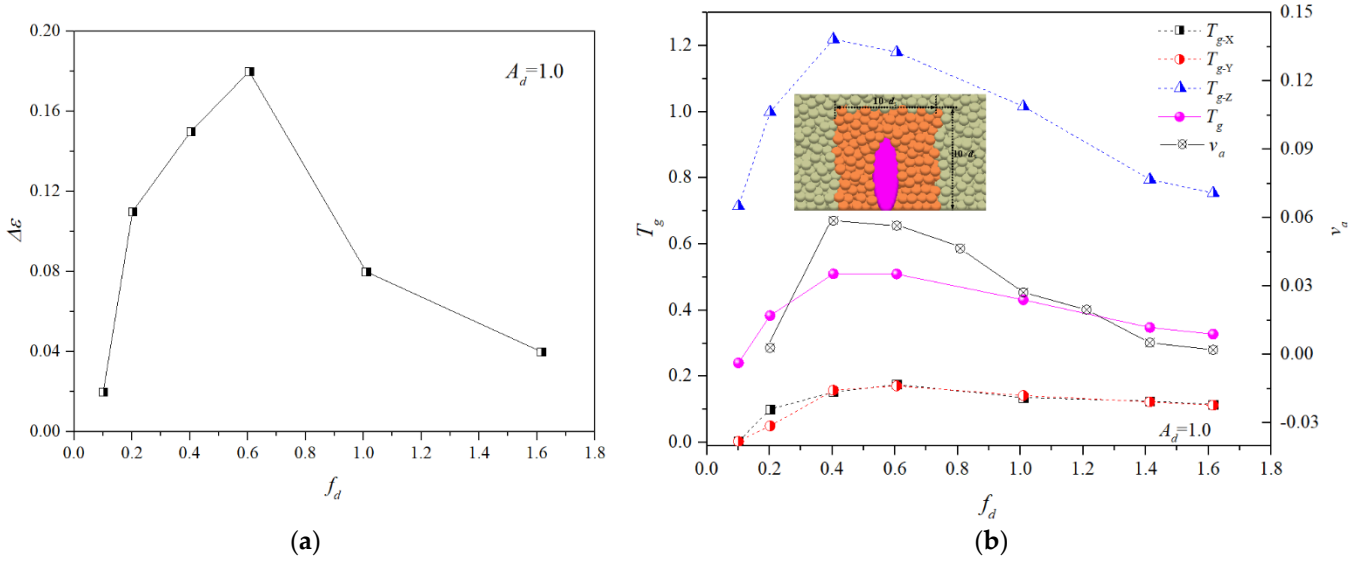

Figure 9. The influence of f on: (**a**) porosity of bed layer at 20·d_s height; (**b**) the granular temperature.

In addition, according to [43], the influence of f_d could also be linked to the change in the external energy input efficiency. The "granular temperature" that has been widely used to describe the kinetics of particle flow is linked with the random motion of particles [44,45]. Here the granular temperature (T_g) in the squared vicinity of the intruder was measured, and T_g is given by [46]

$$T_g = \frac{T_{gx} + T_{gy} + T_{gz}}{3} \tag{7}$$

$$\left\{ \begin{array}{l} T_{gx} = \frac{\sum_{i=1}^{N_i} (v_{ix} - \overline{v_x})^2}{N_i} \\ T_{gy} = \frac{\sum_{i=1}^{N_i} (v_{iy} - \overline{v_y})^2}{N_i} \\ T_{gz} = \frac{\sum_{i=1}^{N_i} (v_{iz} - \overline{v_z})^2}{N_i} \end{array} \right\} \tag{8}$$

where T_{gx}, T_{gy}, and T_{gz} represent the granular temperature in x, y, and z directions, respectively; i refers to the ith particle and N_i is the total number of particles of interest; v_{ix}, v_{iy}, and v_{iz} denote the triaxial velocities of the ith particle and $\overline{v_x}$, $\overline{v_x}$, and $\overline{v_x}$ are ensemble-average velocities, respectively. Figure 9b shows that the variation of T_g with the change of f_d is similar to that of v_a, suggesting a correlation between T_g and v_a. This indicates that an increase of f_d will increase the random motion of small particles, which enhances the filling process and thereupon promotes the percolation.

To the best of our knowledge, for the ascending of a single intruder in a vibrated bed, the non-monotonic dependence of the ascending velocity to vibration frequency has never been reported before. This may be due to the limited range of vibration frequency used in previous studies. For example, in the research by Khan Ahmad [26], only the cases of $f > 50$ Hz were investigated. Additionally, frequencies ranging in 4.07–4.99 Hz were investigated by Liffman et al. [22], who only found a positive effect of f on v_a when A is fixed. On the other hand, some studies only presented the effect of vibration frequency on v_a with fixed Γ [26,31], which simply showed a negative correlation of f on v_a.

These comparisons show that the effects of A and f on v_a are more complicated than previously reported, therefore they can be considered in a wider range and their individual influence can be more carefully examined. Thus, a phase diagram of v_a as a function of A_d and f_d for our simulated results is presented as Figure 10, where the intruder is of d_{Sau} = 6 mm and a/b= 3.0. Note that the cases with extreme large A_d and f_d were not included because the bed oscillates too violently to determine the position of the intruder. It can be seen that the phase diagram shows the symmetrical distribution of v_a with A_d and f_d. Generally, a larger v_a can be obtained when $A_d \in [1.25, 2.0]$ and $f_d < 0.6$. The phase diagram also shows qualitative agreement with the variation trend of v_a against f_d in [31], which reported that ascending velocity decreases with vibration frequency when Γ = 3.83 and Γ = 3.75.

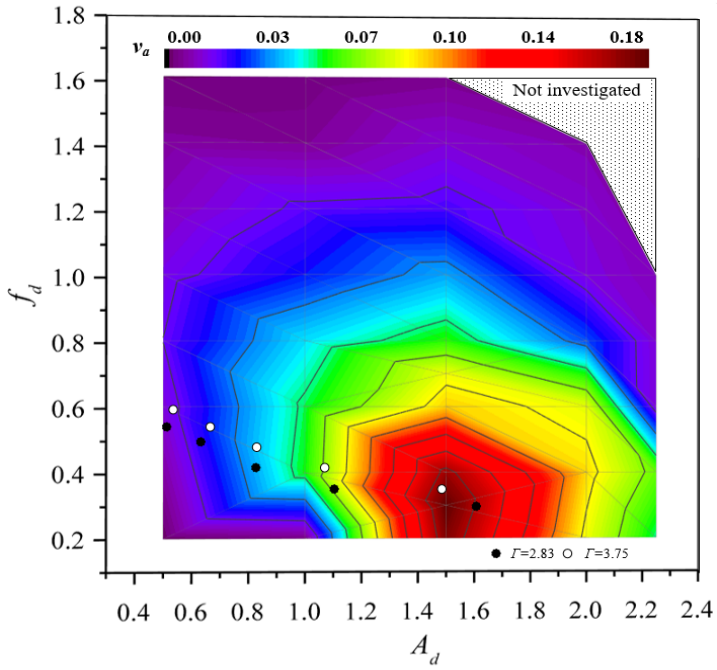

Figure 10. v_a as a function of f_d and A_d for the intruder of d_{Sau} = 6 mm, a/b = 3.0. ○ and ● show the vibration conditions used in [31].

3.3. Modeling of Ascending Velocity

It is shown in the above discussion that the inflection points in non-monotonic response curves (v_a-A and v_a-f) may vary with A and f simultaneously. Thus, before modeling, the critical change condition should be identified first. Several series of data with either A or f varied are selected to be analyzed together, which are listed in Table 4. Previously, Fernando et al. [29] found that for a spherical intruder, the critical change of v_a can be linked with the vibration velocity amplitude V_b, given by $V_b = 2\pi Af(d_s \cdot g)^{-0.5}$. In particular, v_a increases with V_b when $V_b < 2.8$, but decreases with V_b when $V_b > 2.8$. Similarly, the maximum v_a occurs when $V_b = 2.75$ for some of our series of results, as shown in Figure 11a. However, this is not always the case for other simulation results, as shown in Figure 11a.

Instead, it is found that Γ = 4.83 can more uniformly identify the critical change of v_a for our simulation results, as shown in Figure 11b.

Table 4. Parameters used in cases in Figure 11.

No.	f_d	A_d	d_l/d_s	a/b
1	0.40	[0.5, 2.25]	3 (d_{Sau})	2.0
2	0.40	[0.5, 2.25]	3 (d_{Area})	2.0
3	0.40	[0.5, 3.50]	3 (d_{Sau})	4.0
4	0.40	[0.25, 2.25]	3 (d_{Area})	3.0
5	[0.20, 1.61]	0.5	3 (d_{Sau})	3.0
6	[0.20, 1.61]	1.0	3 (d_{Sau})	3.0

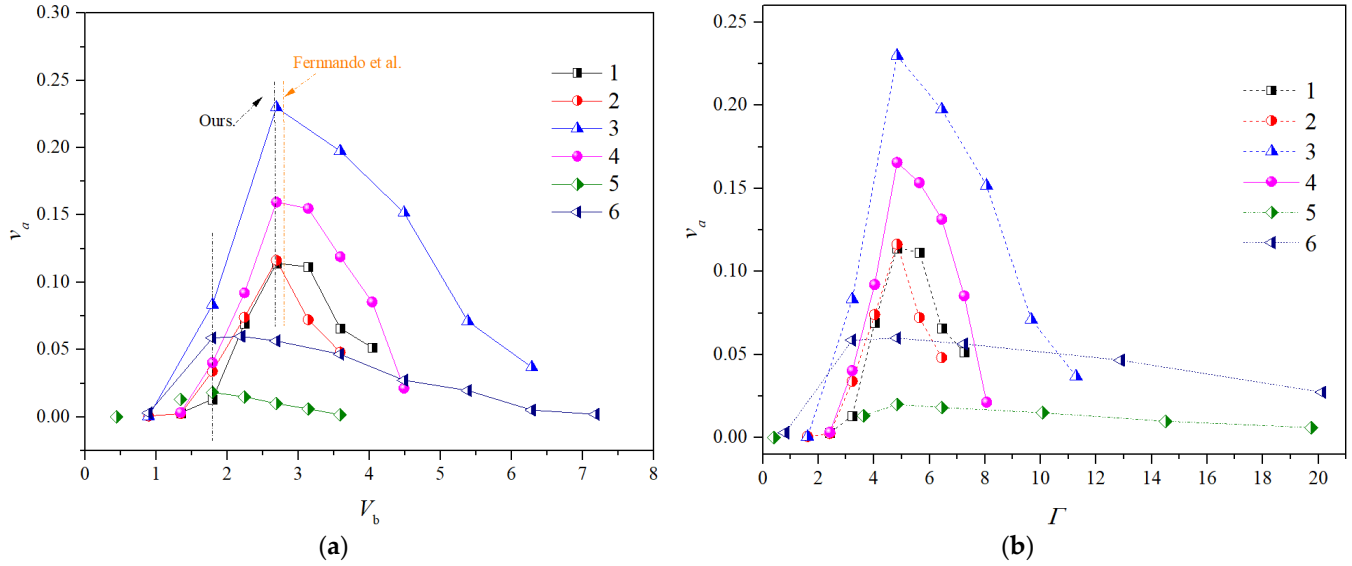

Figure 11. Response of v_a to: (**a**) V_b; (**b**) Γ. The conditions for the curves are listed in Table 4.

Even the critical point at Γ = 4.83 is identified, and one can see that the data points do not collapse into one curve either in Figure 11a,b, indicating both V_b and Γ cannot be used as a single vibration parameter to model v_a. Comparing V_b and Γ, it can be noticed that they are both in proportion to Af^n, but with different n values. Therefore, in our previous study, we have searched n for the best correlation between v_a and $A_d \cdot f_d^{\,n}$ in a binary system of spherical particles, and it was shown that $A_d \cdot f_d^{\,0.5}$ can be used to model v_a uniformly. Here, it is applied to our simulation results and other experiment results. Figure 12 shows that $A_d \cdot f_d^{\,0.5}$ can always be used to uniformly describe v_a for a set of data with different vibration conditions, though the dependency is different in different sets, which should be due to the differences in other parameters, such as different particles used [22,31–33].

In addition, Figure 13a shows that the shape of the intruder has a significant impact on its ascending. This seems to be different from the conclusion in [26] that the shape of the intruder has little effect. The reason is probably because that in the experiments in [26] there was strong convection in the vibrated bed, but in our simulations with PBCs the convection was not formed. In such conditions, the shape of the intruder should be considered. In fact, as shown in Figure 13a, v_a is proportional to Φ^{γ}, where Φ is the sphericity of the intruder and γ is the exponent.

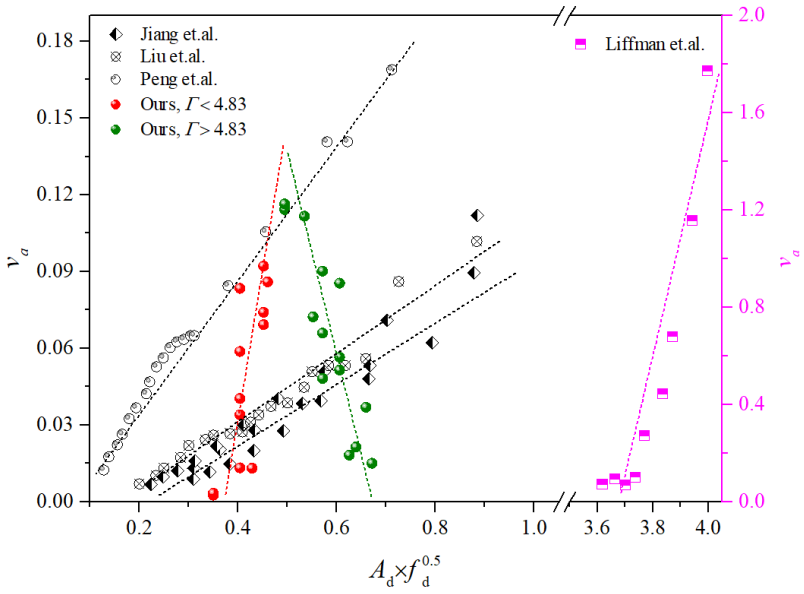

Figure 12. Response of v_a to $A_d \cdot f_d^{0.5}$.

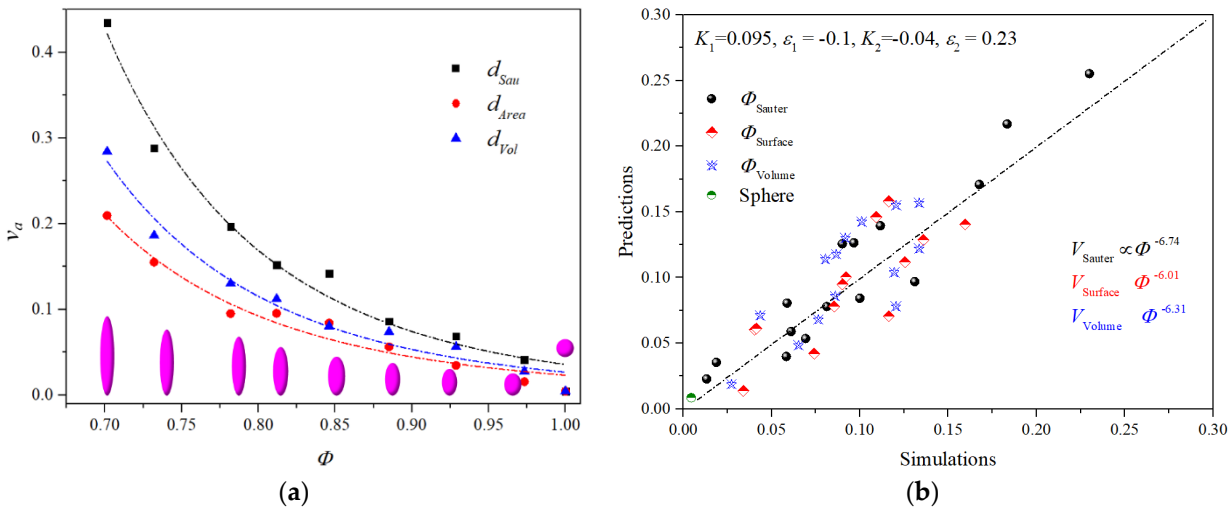

(**a**) (**b**)

Figure 13. (**a**) The response of v_a to the sphericity Φ; (**b**) the predictive values based on Equation (9) against the simulation data.

Based on the above discussion, a model is proposed to predict the ascending velocity of a non-spherical intruder in a vibrated bed of small mono-size spherical particles:

$$v_a = \left\{ \begin{array}{l} K_1 \cdot A_d \cdot f_d^{0.5} \cdot \Phi^{\gamma} + \varepsilon_1, \ \Gamma < 4.83 \\ K_2 \cdot A_d \cdot f_d^{0.5} \cdot \Phi^{\gamma} + \varepsilon_2, \ \Gamma > 4.83 \end{array} \right\} \quad (9)$$

where K_1 and K_2 are proportionality coefficients, ε_1 and ε_2 are correction coefficients, respectively. These coefficients can be fitted for a given granular system. As shown in Figure 13b, the better fitting of our simulation results can be obtained when K_1, K_2, ε_1, and ε_2 are 0.095, −0.04, −0.1, and 0.23, respectively. As the ascending velocity may be changed when using different equivalent diameters, here γ for using d_{Sau}, d_{Area}, and d_{Vol} are respectively given as $\gamma_{\mathrm{Sau}} = -6.74$, $\gamma_{Area} = -6.01$, and $\gamma_{\mathrm{Vol}} = -6.31$. It can be seen that there is a slight difference between γ_{Sau}, γ_{Vol}, and γ_{Area}, and v_a calculated with the same sphericity but different equivalent diameters have the highest value when d_{Sau} is used, while the lowest value when d_{Area} is used.

To further test the model, the experimental results for a single spherical intruder (Φ = 1.0) in [31–33] were also fitted by our Equation (9). The predicted values by the fitting equations were compared to the experimental data in Figure 14. The predictions are in good agreement with the experimental values, showing the model has general applicability.

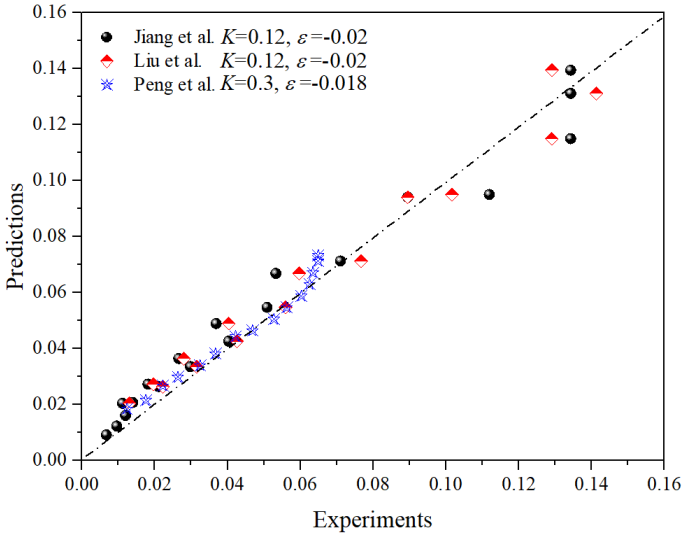

Figure 14. Comparisons of v_a in [31–33] to their predictive value based on Equation (9), Φ = 1.0.

4. Conclusions

In this paper, the segregation of a large intruder of different shapes in a vibrated bed of small particles was investigated by a DEM model. Several important conclusions can be drawn from the results.

Firstly, the ascending velocity (v_a) of a non-spherical intruder increases first and then decreases with the rising of the dimensionless vibration amplitude (A_d). There is a similar variation trend of v_a with increasing dimensionless vibration frequency (f_d). An intruder of larger aspect ratio rises faster under the same vibration conditions.

Secondly, under both the influences of A_d and f_d, the change of the porosity variation of the vibrated bed during a vibration period ($\Delta\varepsilon$) is similar to that of v_a. This indicates that the changes of v_a can be primarily attributed to the change in void filling of small particles, as in our simulations the convection was not generated, and the percolation mechanism dominated the segregation. This can also be used to explain the effect of intruder shape, as a more elongated intruder can make void filling more efficient, resulting in a larger v_a. The change of granular temperature (T_g) also shows a link to the change of v_a.

Thirdly, not only for current simulations but also for the experimental data in the literature, $A_d \cdot f_d^{0.5}$ is shown to be an appropriate combined parameter to characterize the influence of A and f on v_a. Additionally, v_a is related to the negative nth power of the intruder's sphericity Φ. Based on these findings, a piecewise equation has been proposed to model v_a as a function of A_d, f_d, and Φ. The equation can be well fitted with all our simulation results and the experimental results in the literature. The coefficients in the equation are dependent on other particle properties, which deserve further study.

Author Contributions: Conceptualization, J.Q. and K.D.; methodology, J.Q. and C.D.; software, J.Q. and C.D.; validation, J.Q. and K.D.; formal analysis, J.Q. and K.D.; investigation, J.Q.; resources, J.Q.; data curation, J.Q., C.D., and K.D.; writing—original draft preparation, J.Q.; writing—review and editing, K.D.; visualization, J.Q., C.D., and K.D.; supervision, C.D. and K.D.; project administration, C.D.; funding acquisition, C.D. All authors have read and agreed to the published version of the manuscript.

Funding: This research was funded by the joint Ph.D. program of "double first rate" construction disciplines of CUMT.

Institutional Review Board Statement: Not applicable.

Informed Consent Statement: Not applicable.

Data Availability Statement: The data presented in this study are available on request from the corresponding author. The data are not publicly available due to the protection of ongoing original research.

Acknowledgments: The first author thanks Western Sydney University and ARC Hub for Computational Powder Technology for hosting his visit.

Conflicts of Interest: The authors declare no conflict of interest.

References

1. Shinbrot, T.; Shinbrot, T. Granular materials: The Brazil nut effect–in reverse. *Nature* **2004**, *429*, 352–353. [CrossRef]
2. Breu, A.; Ensner, H.M.; Kruelle, C.A.; Rehberg, I. Reversing the Brazil-nut effect: Competition between percolation and condensation. *Phys. Rev. Lett.* **2003**, *90*, 143021. [CrossRef]
3. Williams, J.C.; Shields, G. The segregation of granules in a vibrated bed. *Powder Technol.* **1967**, *1*, 134–142. [CrossRef]
4. Rosato, A.; Strandburg, K.J.; Prinz, F.; Swendsen, R.H. Why the Brazil nuts are on top: Size segregation of particulate matter by shaking. *Phys. Rev. Lett.* **1987**, *58*, 1038–1040. [CrossRef]
5. Walliser, H. Comment on "Reverse Brazil Nut Problem: Competition between Percolation and Condensation". *Phys. Rev. Lett.* **2001**, *89*, 189603. [CrossRef]
6. Möbius, M.E.; Lauderdale, B.E.; Nagel, S.R.; Jaeger, H.M. Brazil-nut effect: Size separation of granular particles. *Nature* **2001**, *414*, 270. [CrossRef]
7. Huerta, D.A.; Ruiz-Suárez, J.C. Vibration-Induced Granular Segregation: A Phenomenon Driven by Three Mechanisms. *Phys. Rev. Lett.* **2004**, *92*, 114301. [CrossRef]
8. Duran, J.; Rajchenbach, J.; Clément, E. Arching effect model for particle size segregation. *Phys. Rev. Lett.* **2003**, *70*, 2431–2434. [CrossRef]
9. Yan, X.; Shi, Q.; Hou, M.; Lu, K.; Chan, C.K. Effects of Air on the Segregation of Particles in a Shaken Granular Bed. *Phys. Rev. Lett.* **2003**, *91*, 14302. [CrossRef]
10. Shinbrot, T.; Muzzio, F.J. Reverse Buoyancy in Shaken Granular Beds. *Phys. Rev. Lett.* **1998**, *81*, 4365–4368. [CrossRef]
11. Nahmad-Molinari, Y.; Canulchay, G.; Ruizsuárez, J.C. Inertia in the Brazil nut problem. *Phys. Rev. E* **2003**, *68*, 352–375. [CrossRef] [PubMed]
12. Vanel, L.; Rosato, A.D.; Dave, R.N. Rise-Time Regimes of a Large Sphere in Vibrated Bulk Solids. *Phys. Rev. Lett.* **1997**, *78*, 1255–1258. [CrossRef]
13. Tai, C.H.; Hsiau, S.S.; Kruelle, C.A. Density segregation in a vertically vibrated granular bed. *Powder Technol.* **2010**, *204*, 255–262. [CrossRef]
14. Lim, E.W.C. Density segregation in vibrated granular beds with bumpy surfaces. *AICHE J.* **2010**, *56*, 2588–2597. [CrossRef]
15. Shi, Q.; Sun, G.; Hou, M.; Lu, K. Density-driven segregation in vertically vibrated binary granular mixtures. *Phys. Rev. E Stat. Nonlin. Soft Matter Phys.* **2007**, *75*, 61302. [CrossRef] [PubMed]
16. Jain, A.; Metzger, M.J.; Glasser, B.J. Effect of particle size distribution on segregation in vibrated systems. *Powder Technol.* **2013**, *237*, 543–553. [CrossRef]
17. Krouskop, P.E.; Talbot, J. Studies of Mass and Size Effects in Three-Dimensional Vibrofluidized Granular Mixtures. *Phys. Rev. E Stat. Nonlin. Soft Matter Phys.* **2003**, *68*, 21304. [CrossRef]
18. Haff, P.K.; Werner, B.T. Computer simulation of the mechanical sorting of grains. *Powder Technol* **1986**, *48*, 239–245. [CrossRef]
19. Schröter, M.; Swinney, H.L.; Ulrich, S. Influence of friction on granular segregation. *Phys. Rev. E* **2007**, *76*, 42301.
20. Bose, M.; Rhodes, M. Dynamics of an intruder in a shaken granular bed. *Powder Technol.* **2007**, *179*, 25–30. [CrossRef]
21. Rosato, A.; Prinz, F.; Strandburg, K.J.; Swendsen, R.H. Monte Carlo Simulation of Particle Matter Segregation. *Powder Technol.* **1986**, *49*, 59–69. [CrossRef]
22. Liffman, K.; Muniandy, K.; Rhodes, M.; Gutteridge, D.; Metcalfe, G. A segregation mechanism in a vertically shaken bed. *Granul. Matter* **2001**, *3*, 205–214. [CrossRef]
23. Knight, J.B.; Jaeger, H.M.; Nagel, S.R. Vibration-induced size separation in granular media—The convection connection. *Phys. Rev. Lett.* **1993**, *70*, 3728–3731. [CrossRef]
24. Hirt, C. Size Segregation and Convection. *Europhys. Lett.* **1995**, *29*, 123–128.
25. Burtally, N.; King, P.J.; Swift, M.R.; Leaper, M. Dynamical behaviour of fine granular glass/bronze mixtures under vertical vibration. *Granul. Matter* **2003**, *5*, 57–66. [CrossRef]
26. Ahmad, K.; Smalley, I.J. Observation of particle segregation in vibrated granular systems. *Powder Technol.* **1973**, *8*, 69–75. [CrossRef]
27. Kock, I.; Huhn, K. Influence of particle shape on the frictional strength of sediments—A numerical case study. *Sediment Geol.* **2007**, *196*, 217–233. [CrossRef]

28. Jha, A.K.; Gill, J.S.; Puri, V.M. Percolation Segregation in Binary Size Mixtures of Spherical and Angular-Shaped Particles of Different Densities. *Part. Sci. Technol.* **2008**, *26*, 482–493. [CrossRef]
29. Fernando, D.N.; Wassgren, C.R. Effects of vibration method and wall boundaries on size segregation in granular beds. *Phys. Fluids* **2003**, *15*, 3458. [CrossRef]
30. Hsiau, S.; Yu, H. Segregation phenomena in a shaker. *Powder Technol.* **1997**, *93*, 83–88. [CrossRef]
31. Jiang, Z.; Jing, Y.; Zhao, H.; Zheng, R. Effects of subharmonic motion on size segregation in vertically vibrated granular materials. *Acta Phys. Sin.* **2009**, *58*, 5923–5929.
32. Liu, Y.; Zhao, J. A model for the Brazil-nut segregation time. *Granul. Matter* **2015**, *17*, 265–270. [CrossRef]
33. Peng, Y.; Zhang, Z.; Wang, Y.; Liu, X. Experimental and theoretical investigations of the effect of "Brazil Nut" segregation in vibrating granular matters. *Acta Phys. Sin.* **2012**, *61*, 279–286.
34. Qiao, J.; Wen, P.; Duan, C.; Wang, W. Particle behavior and parameter optimization in treatment of waste petroleum reforming catalysts based on a compound dry separator. *Adv. Powder Technol.* **2020**, *31*, 1181–1195. [CrossRef]
35. Qiao, J.; Huang, L.; Duan, C.; Jiang, H.; Zhao, Y.; Shao, H.; Pan, M. Research on separation mechanism of waste palladium catalyst in a structure-optimized compound dry separator based on DEM-CFD. *Part. Sci. Technol.* **2020**, *38*, 131–143. [CrossRef]
36. Qiao, J.; Duan, C.; Jiang, H.; Zhao, Y.; Chen, J.; Huang, L.; Wen, P.; Wu, J. Research on screening mechanism and parameters optimization of equal thickness screen with variable amplitude based on DEM simulation. *Powder Technol.* **2018**, *331*, 296–309. [CrossRef]
37. Dong, K.; Esfandiary, A.H.; Yu, A.B. Discrete particle simulation of particle flow and separation on a vibrating screen: Effect of aperture shape. *Powder Technol.* **2017**, *314*, 195–202. [CrossRef]
38. Liu, C.; Wang, H.; Zhao, Y.; Zhao, L.; Dong, H. DEM simulation of particle flow on a single deck banana screen. *Int. J. Min. Sci. Technol.* **2013**, *23*, 273–277. [CrossRef]
39. Elperin, T.; Golshtein, E. Effects of convection and friction on size segregation in vibrated granular beds. *Phys. A Stat. Mech. Its Appl.* **1997**, *247*, 67–78. [CrossRef]
40. Qiao, J.; Duan, C.; Dong, K.; Wang, W.; Jiang, H.; Zhu, H.; Zhao, Y. DEM study of segregation degree and velocity of binary granular mixtures subject to vibration. *Powder Technol.* **2021**, *382*, 107–117. [CrossRef]
41. Amirifar, R.; Dong, K.; Zeng, Q.; An, X. Self-assembly of granular spheres under one-dimensional vibration. *Soft Matter* **2018**, *18*, 9856–9869. [CrossRef]
42. Amirifar, R.; Dong, K.; Zeng, Q.; An, X. Bimodal self-assembly of granular spheres under vertical vibration. *Soft Matter* **2019**, *15*, 5933–5944. [CrossRef]
43. Hu, K.; Xie, Z.A.; Wu, P.; Sun, J.; Li, L.; Jia, C.; Zhang, S.; Liu, C.; Wang, L. Convecting particle diffusion in a binary particle system under vertical vibration. *Soft Matter* **2014**, *10*, 4348–4359. [CrossRef]
44. Wildman, R.D.; Huntley, J.M. Novel method for measurement of granular temperature distributions in two-dimensional vibro-fluidised beds. *Powder Technol.* **2000**, *113*, 14–22. [CrossRef]
45. Tai, C.H.; Hsiau, S.S. Dynamic behaviors of powders in a vibrating bed. *Powder Technol.* **2004**, *139*, 221–232. [CrossRef]
46. Hsiau, S.S.; Lu, L.S.; Tai, C.H. Experimental investigations of granular temperature in vertical vibrated beds. *Powder Technol.* **2008**, *182*, 202–210. [CrossRef]